Environmental Science & Technology

pubs.acs.org/est

Article

Eight-Year Estimates of Methane Emissions from Oil and Gas Operations in Western Canada Are Nearly Twice Those Reported in Inventories

Elton Chan, Douglas E. J. Worthy,* Douglas Chan, Misa Ishizawa, Michael D. Moran, Andy Delcloo, and Felix Vogel

Cite This: *Environ. Sci. Technol.* 2020, 54, 14899−14909

Read Online

ACCESS | Metrics & More | Article Recommendations | Supporting Information

ABSTRACT: The provinces of Alberta and Saskatchewan account for 70% of Canada's methane emissions from the oil and gas sector. In 2018, the Government of Canada introduced methane regulations to reduce emissions from the sector by 40−45% from the 2012 levels by 2025. Complementary to inventory accounting methods, the effectiveness of regulatory practices to reduce emissions can be assessed using atmospheric measurements and inverse models. Total anthropogenic (oil and gas, agriculture, and waste) emission rates of methane from 2010 to 2017 in Alberta and Saskatchewan were derived using hourly atmospheric methane measurements over a six-month winter period from October to March. Scaling up the winter estimate to annual indicated an anthropogenic emission rate of 3.7 ± 0.7 $MtCH_4$/year, about 60% greater than that reported in Canada's National Inventory Report (2.3 $MtCH_4$). This discrepancy is tied primarily to the oil and gas sector emissions as the reported emissions from livestock operations (0.6 $MtCH_4$) are well substantiated in both top-down and bottom-up estimates and waste management (0.1 $MtCH_4$) emissions are small. The resulting estimate of 3.0 $MtCH_4$ from the oil and gas sector is nearly twice that reported in Canada's National Inventory (1.6 $MtCH_4$).

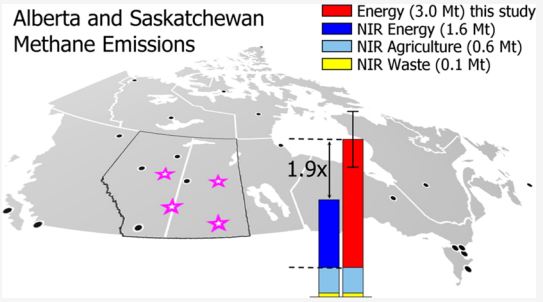

INTRODUCTION

Methane is a short-lived greenhouse gas and is 25−34 times more potent than carbon dioxide on a 100-year time horizon and 96 times more potent over a 20-year time horizon.[1] Near-term reductions in methane emissions will have a larger short-term impact on changes in global temperatures and are a key to limiting climate change temperatures to well below 2 °C.[2] In 2018, the Government of Canada finalized national regulations to reduce methane emissions from the oil and gas sector by 40 to 45 percent from the 2012 levels by 2025.[3,4] In Canada, Alberta and Saskatchewan provinces account for 70% of methane emissions from the oil and gas sector, primarily from the production and processing of crude oil and natural gas.[5]

National inventory reporting follows the Intergovernmental Panel on Climate Change (IPCC) methodologies.[6] To date, results from independent atmospheric approaches are rarely considered as additional sources of information for national inventory reporting. However, the revised 2019 methodology report recognizes the importance of verification systems based on observations and modeling that are in line with priorities for inventory development.[7] A number of studies in the United States have documented methane emissions from oil and natural gas activities to be systematically higher than those reported in inventories.[8−16] Recent studies in Alberta have yielded similar results for specific regions.[17−20] For example, airborne measurements of methane from a series of flights conducted during October 27 to November 5, 2016 near the Red Deer (50 km × 50 km) and Lloydminster (60 km × 60 km) areas found the airborne measurement-derived flux results to be 17 and 5 times greater than the emissions derived from direct reported data for Red Deer and Lloydminster, respectively. In comparison to the region-specific bottom-up inventory-based estimate, the results for the Red Deer area were consistent with the airborne measurement-derived flux results; however, for the Lloydminster area, the airborne measurement-derived flux results were four times greater than their bottom-up inventory-based estimate. Although the scaling of results from these limited study regions, in both spatial extent and time, to provincial totals may introduce large uncertainties, they do indicate the potential for larger emissions from the oil and gas sector than are currently reported in the national inventory.

The combination of high-frequency hourly atmospheric greenhouse gas measurements from strategically located tower

Received: June 23, 2020
Revised: October 26, 2020
Accepted: October 30, 2020
Published: November 10, 2020

sites, which limits impacts of local sources, with inverse methods and atmospheric transport models can be used to quantify regional greenhouse gas emissions. Atmospheric inversion modeling systems have been widely used to estimate greenhouse gas emissions in Europe[21−30] and in the United States.[13,31−35] In this study, we have applied an ensemble regional inverse modeling framework to quantify methane emissions from 2010 to 2017 for Alberta and Saskatchewan using atmospheric measurements of methane from two sites in Alberta and two sites in Saskatchewan over a six-month winter period from October to March when wetland emissions are low. Unlike the previously noted smaller spatiotemporal scale studies conducted in Alberta, the regional atmospheric ensemble inversion framework employed here covers the entire combined area of Alberta and Saskatchewan (approximately 10° latitude by 20° longitude) and extends over eight winters.

This paper is organized as follows. The Materials and Methods section presents (1) the methane observations and a back trajectory analysis illustrating the relationship of the CH_4 measurement variability to the emission spatial distribution surrounding the measurement sites and (2) the description of the regional inversion model and model performance evaluation. The Inversion Results and Discussion section focuses on methane emission estimates from our inversion model and the comparison of these emissions with inventory-based emissions, then ending with some discussions of the implications of this study.

MATERIALS AND METHODS

Methane Observations. For this inversion work, atmospheric methane observations over the period from 2010 to 2017 from two sites located in Alberta, Lac La Biche (LLB) and Esther (EST), and two sites in Saskatchewan, East Trout Lake (ETL) and Bratt's Lake (BRA), were used. A map showing the locations of the sites and the study domain is shown in Figure S1. Site descriptions and details of instrumentation, sampling, calibration, data collection, and data processing are provided in the Supporting Information (S.1 and S.2). Figure 1 shows the time series of hourly averaged methane from ETL, LLB, BRA, and EST for January 2016, illustrating typical temporal variability in atmospheric methane concentrations at these four sites in winter. The full time series of hourly averaged atmospheric methane from ETL, LLB, BRA, and EST for the period from January 1, 2010, to December 31, 2017, is shown in Figure S2. Also shown in Figure 1 is the corresponding methane time series from Alert, Nunavut, located on the northeastern tip of Ellesmere Island in the Canadian Arctic (Figure S1). Alert is far removed from large industrial regions in the Northern Hemisphere; hence, its methane time series provides a measure of the variation that is typically observed at a remote site that is not influenced by local or regional sources.[36] The episodic events (or peaks) in methane observed at ETL, LLB, BRA, and EST shown in Figure 1 are synoptic in nature and tend to last 2 to 5 days. These events are due to regional anthropogenic methane sources (oil and gas, agriculture, and waste management) and prevailing meteorological conditions, specifically wind direction and planetary boundary layer (PBL) depth. In winter, the cold surface induces shallow PBL (the well-mixed layer above the surface) conditions, allowing methane near the surface to accumulate over several consecutive days. As a result, the transport of methane-enriched air masses from source regions to the measurement sites results in higher atmospheric methane levels. The variability is unique at each site reflecting the relative proximity of sources to the site and the wind direction, which determines whether the sources are upwind of the site. The larger variability observed at LLB and EST relative to ETL and BRA reflects that LLB and EST are closer to strong methane sources. The observed short-term variability starts to diminish by the middle of March, and by April, the time series of methane is much less variable due to the convective surface layer being more active (with more solar heating) resulting in a higher PBL. The reduced short-term variability (i.e., lack of signal) in spring and the addition of wetland methane emissions preclude the usefulness of this data to specifically reflect the anthropogenic source behavior. Although these fluxes could be modeled in all months, the introduction of wetland emissions in inversion modeling frameworks would introduce additional large uncertainties in this analysis.[27,28,37−39] Wetlands are the largest source of methane in Alberta and Saskatchewan in mid-summer but a near zero source in mid-winter.[27,28,37−39]

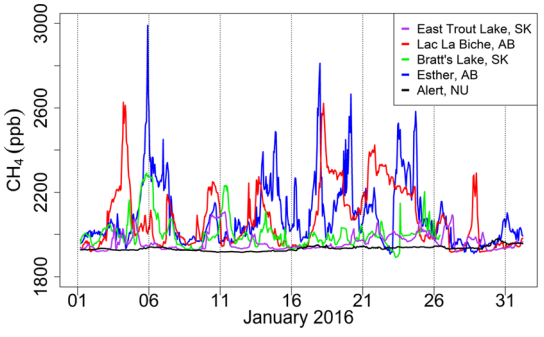

Figure 1. Time series of hourly averaged methane dry air mole fractions at Bratt's Lake, SK, Esther, AB, Lac La Biche, AB, East Trout Lake, SK, and Alert, NU, for the period from January 1 to January 31, 2016. Time series data from Alert, located on the northeastern tip of Ellesmere Island in the Canadian Arctic, illustrate the variation typically observed at a remote background site.

Back Trajectory Analysis of Source Regions Impacting Methane Variability. Canada's National Inventory Report (NIR)[5] provides contributions of methane sources in Alberta and Saskatchewan for energy, primarily oil and gas (70%), agriculture (25%), and waste management (5%). Shown in Figure 2a are the locations of individual active oil and natural gas wells (from 2013 to 2016) to provide a visual reference of the spatial distribution of potential oil and gas sources in Alberta and Saskatchewan. Forty percent (~5 million) of Canada's 12 million cattle[40] is located in Alberta. Approximately 70% (~3.5 million) of Alberta's total cattle (including both grazing and feedlot cattle) is distributed within the red oval shown in Figure 2a. Twenty percent (~2.5 million) of Canada's cattle population is located in Saskatchewan and is generally evenly distributed throughout the lower half of the province.[40] As the waste source emissions are small, they have not been included in Figure 2a.

To demonstrate that the variation in atmospheric methane reflects differences in air mass origin, atmospheric transport pathways with the distribution of methane sources are shown in Figure 2c. For example, in Figure 2b, the 21 UTC (15:00 local standard time) hourly methane values from November 1, 2015, to February 28, 2016, at LLB have been plotted by color,

https://dx.doi.org/10.1021/acs.est.0c04117
Environ. Sci. Technol. 2020, 54, 14899−14909

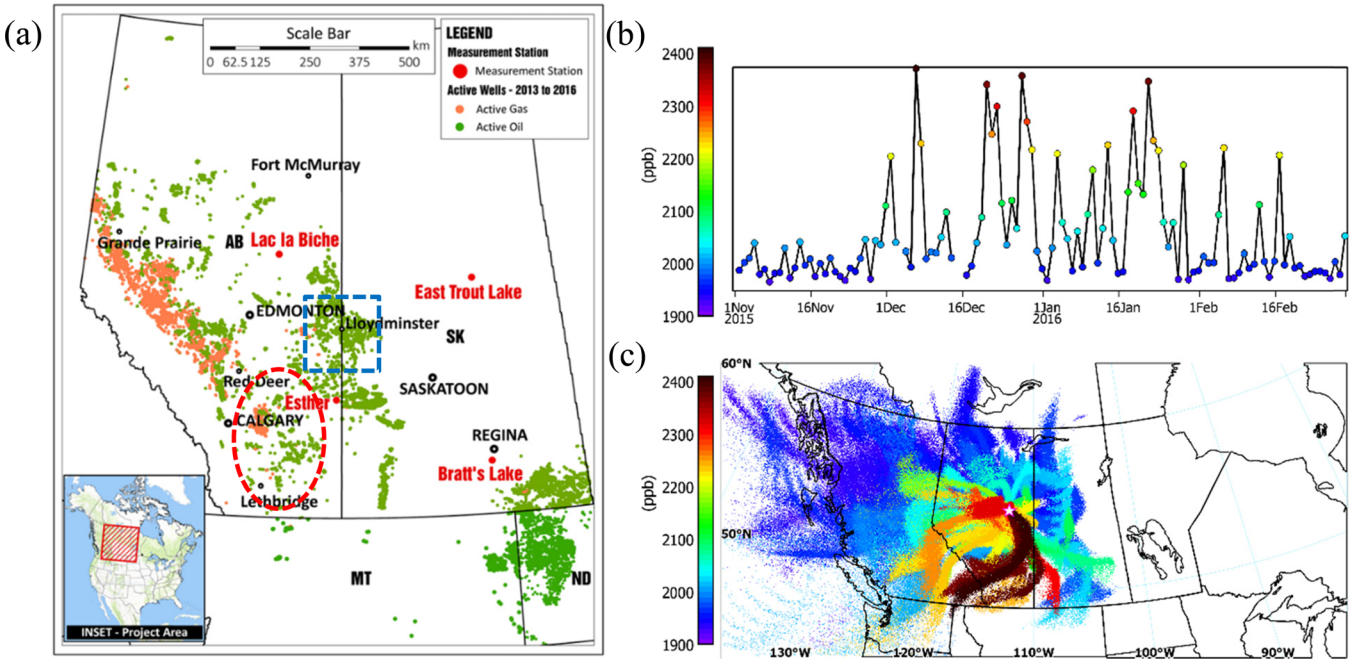

Figure 2. (a) Map of western Canada showing the location of LLB, EST, BRA, and ETL (in red text) along with the distribution of active oil and gas wells from 2013 through 2016. The area in the blue box shows the CHOPS geographical region. The area within the red oval shows the primary agricultural region in Alberta. (b) Methane (21 UTC or 15:00 local standard time) mole fraction values observed at LLB from November 1, 2015, to February 28, 2016, associated with (c) 36 h backward air parcel trajectories for LLB with heights within the near-surface layer (0−100 m above ground) using identical colors to identify mole fraction magnitudes.

with brown and red representing high mole fractions and lower mole fractions shown in blue and green. The transport pathway for each daily 21 UTC hourly value (Figure 2c) is generated using 36 h backward air parcel trajectories from the dispersion model of FLEXPART[41] and mapped using the color associated with the 21 UTC hourly data value.

Close examination of Figure 2b,c reveals high variability in the methane data record associated with various transport directions. Higher mole fractions appear to originate from the southeast direction, a well-known cold heavy oil production with sand (CHOPS) geographical region with thousands of active oil wells shown as green dots contained within the blue box shown in Figure 2a. The CHOPS region has been documented to have potentially high fugitive sources of methane due to leaks or venting processes.[5,8,10,15,42−44] Many of the mid-range peaks originate from west and southwest of LLB. Qualitatively, this analysis shows that the source regions shown in Figure 2a indeed influence the variability (the episodic peaks) of methane at the LLB measurement site. The same analysis was conducted for the other three sites, which yielded similar results (not shown).

Regional Inversion Model. In this study, a regional Bayesian inversion model was used to estimate methane emissions for Alberta and Saskatchewan. A detailed description and a flowchart (Figure S3) of the model are provided in the Supporting Information. Only a brief summary is given here.

Bayesian inversion modeling begins with an initial estimate of the spatial emission (prior emissions from an existing inventory database) as an input to an atmospheric transport model to simulate a methane data record. The modeled data are compared to observations to calculate model−observation differences. These differences are then processed using an optimization procedure to estimate the emissions (posterior emissions) that would yield the best match to the observations.

The main components of the inverse modeling framework are (1) an atmospheric transport model, (2) prior emissions, and (3) the optimization procedure. An ensemble has been created to calculate multiple inverse emission estimates using different transport models, different prior emissions, and different optimization setups to provide a more inclusive estimate of the variations or uncertainties possible in the results.

(1) Two independent Lagrangian atmospheric models (see Supporting Information S.3), the FLEXible PARTicle dispersion model (FLEXPART) v8.2[41] and the Stochastic Time-Inverted Lagrangian Transport Model (STILT),[45,46] were used to simulate CH_4 mole fractions. The FLEXPART v8.2[41] model was driven by globally gridded reanalysis meteorology from the European Centre for Medium-Range Weather Forecasts (ECMWF) ERA-Interim (ERA)[47,48] with a horizontal resolution of 1° × 1° for the years 2010−2017. STILT was driven by forecast meteorological fields from the Weather Research and Forecasting model (WRF)[49] with horizontal resolutions of 10 × 10 km and 1° × 1°. The STILT model results were provided by NOAA Carbon-Tracker-Lagrange[50] for the years 2010−2015. Model outputs were generated daily at 21:00 UTC (14:00 or 15:00 LST) representing the well-mixed afternoon conditions near the surface (Figure S4). The boundary conditions (see Supporting Information S.4) for these regional models were taken from the National Institute for Environmental Studies (NIES) global model.[51] Since transport errors can affect the results of the inversion model, having multiple model transports in the ensemble can provide estimates of uncertainties of the posterior emission including potential transport errors.

https://dx.doi.org/10.1021/acs.est.0c04117
Environ. Sci. Technol. 2020, 54, 14899−14909

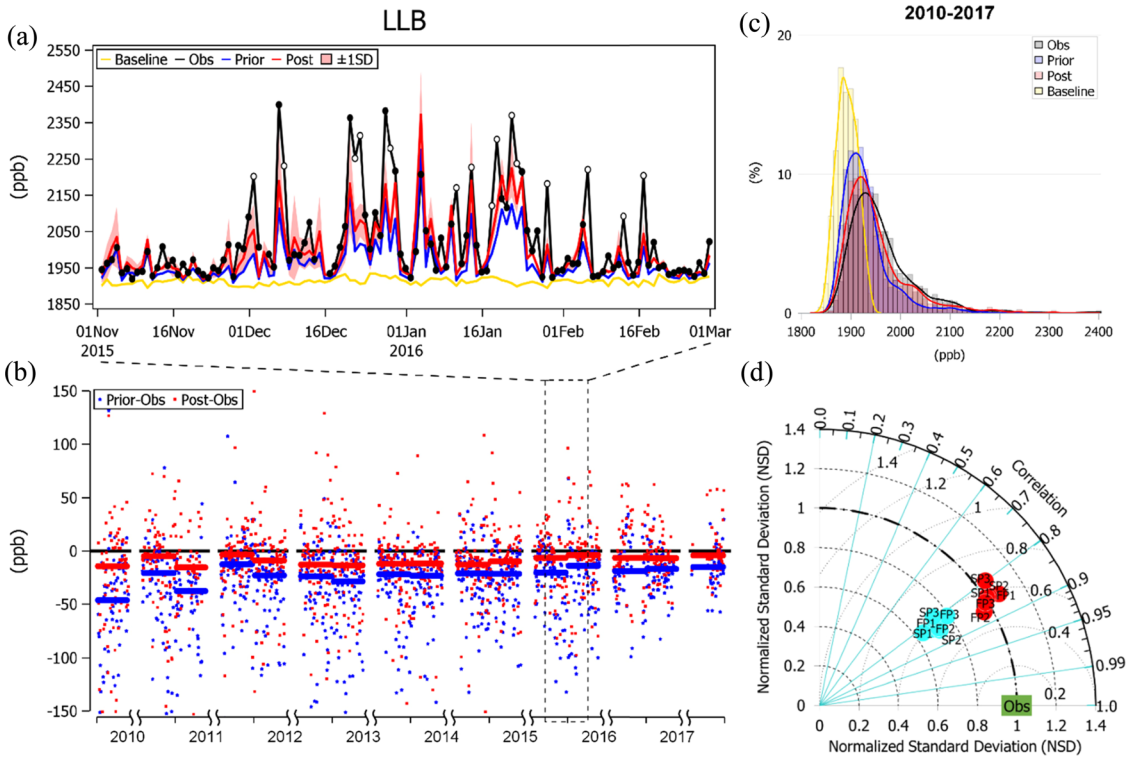

Figure 3. (a) Example period (Nov 1, 2015—Feb 29, 2016) of atmospheric methane observation (black), modeled prior (blue), and posterior (red) time series using the seven-subregion configuration for the LLB site. Methane data values excluded in the inversions are displayed using open circles. One standard deviation (SD) calculated from the ensemble of model runs are shown as pink shaded areas. The modeled methane baseline is shown in yellow. (b) Daily prior-data and posterior-data mismatches for the LLB site are shown using blue and red dots, respectively. Corresponding medians for the 16 individual three-month time periods are shown using horizontal lines. The dashed rectangle represents the corresponding time series analysis shown in (a). (c) Statistical distribution of the observation (with data filtering), modeled prior, posterior, and baseline data for 2010–2017. (d) Taylor diagram showing the comparison of the prior (blue circles) and posterior (red circles) simulated methane emissions with the observations from 2010 through 2015 (January—March and October—December) at LLB. F and S refer to FLEXPART and STILT. P1, P2, and P3 refer to the priors.

(2) Three different anthropogenic prior emissions (Table S1) were included in the inversion ensemble to assess the effects of prior emission differences. The time period of our analysis was limited to the colder temperature conditions (October to March) when natural emissions from wetlands and other natural sources (geological seeps, wildfires, and termites) are negligible in Alberta and Saskatchewan,[52,53] thus allowing direct estimates of anthropogenic methane emissions. The anthropogenic prior emissions include oil and gas industrial activities (extraction, processing, etc.) and agriculture (enteric fermentation and manure management) and waste management sources (landfills). The first prior (see Supporting Information S.5) (P1) AQ2013 is compiled by ECCC and scaled to the NIR sectoral totals. Briefly the CH_4 emissions are derived from the volatile organic compound (VOC) inventory in criteria air contaminant (CAC)[54−57] inventories using the ratios of total organic gases (TOGs) to VOC and TOG chemical speciation profiles. See Supporting Information S.9 for the detailed description. The second prior (P2) obtained from the work of Sheng et al.[58] accounts for oil and gas sources, with remaining sources shared from P1, and finally, the third prior (P3) is the global inventory Emission Database for Global Atmospheric Research (EDGAR) v4.2.[59] Further details and comparisons of all three priors (P1, P2, and P3) are given in the Supporting Information.

(3) The Bayesian inversion scheme (Supporting Information S.8) is a minimization procedure to optimize the agreement between the observation and model results. The optimization was resolved in space and time. The scaling factors for subregions were estimated for two time steps (October−December and January−March, three-month interval) per year for eight years. Total emissions of methane were estimated in the subregions in Alberta and Saskatchewan. Two preprocessing steps before inversions were performed and are described as follows: first, baseline-subtracted observations (Supporting Information S.4) were calculated for each site. In addition to the site-specific baseline, any remaining contributions from outside of Alberta and Saskatchewan but within the five-day integration period were subtracted from the observations for each site. The outer-region source contributions to the synoptic variability are less than 10% for the sites used in the inversions. This is followed by a data selection procedure (Supporting Information S.7) to remove large model−observation mismatches.

The subregion spatial configurations were strategically designed to group and separate the main source regions in the prior emission map. In this study, a seven- and a four-subregion spatial configuration were used (Figure S7). The

https://dx.doi.org/10.1021/acs.est.0c04117
Environ. Sci. Technol. 2020, 54, 14899−14909

minimization used was the Markov Chain Monte Carlo (MCMC)[60] method (see Supporting Information S.8) to estimate the optimum (posterior) emissions and uncertainties. A simple linear regression model is then used to calculate the scaling factors. The linear scaling factors λ_p for the subregions for each three-month inversion period of January−March and October−December in Alberta and Saskatchewan for 2010−2017 using FLEXPART and for 2010−2015 using STILT models are estimated to fit the baseline-subtracted observations $y_{t,s}$ according to eq 1

$$y_{t,s} = \sum_{p \in R_T} \lambda_p \left\{ \sum_{g \in G_p} M_{g,p,t,s} x_{g,p,t} \right\} + \epsilon_{t,s} \quad (1)$$

where t is the time of the measurement taken, s is the observational site, and p is the subregion containing the site s. λ_p and model−observation mismatch $\epsilon_{t,s}$ are assumed to follow $N(1, \sigma^2_{prior})$ and $N(0, \sigma^2_{\epsilon})$, respectively. N is the notation for normal distribution. The quantity in {} is the modeled mole fraction for site s at time t from CH_4 emissions in the subregion p. In particular, $x_{g,p,t}$ is the gridded total CH_4 emission field over the subregion p at time t. $M_{g,p,t,s}$ is the site-specific emission sensitivity (Supporting Information S.3) over the subregion p for each grid cell g. R_T is the total number of subregions and G_p is the total number of grid cells in the subregion p. The model−observation mismatches ($\epsilon_{t,s}$) are minimized by optimally adjusting λ_p. The definitions of σ^2_{prior} and σ^2_{ϵ} are provided in the Supporting Information S.8. After the scaling factors had been calculated using eq 1, three-monthly total CH_4 emission estimates (anthropogenic and wetland) for Alberta and Saskatchewan were calculated using equation S.4.

In warmer months, emissions of methane from wetlands, particularly in mid-summer, are significantly higher than anthropogenic emissions, making the partitioning of the anthropogenic sources less certain in the inversion model. Results from April to September are not included in this analysis. Wetland emissions were obtained from a global model of Carbon Tracker Europe-CH_4.[39] These modeled methane emissions from wetlands[39] in October and November in Alberta and Saskatchewan were subtracted from the three-monthly total methane emissions estimated using the above inversion procedure to yield an estimate of the anthropogenic methane emissions. Note that modeled wetland emissions from December to March are near zero. Adjustments for wetland emissions in the late fall are on the order of 5% of the total methane emission estimate in this study. Annual values for 2010−2017 are reported by doubling the results from January to March and October to December since anthropogenic methane emissions from livestock operations and oil and gas production show small seasonal dependencies.[61−64]

The different permutations of transport models, prior emissions, and subregion masks yield an ensemble of 18 posterior emission estimates and their uncertainties. Before discussing the inversion results and their comparison to NIR in the Inversion Results and Discussion section, the following section presents the analysis of the model performance.

Performance of the Inversion System to Minimize the Model−Data Mismatch. Figure 3 shows an example performance metric of the prior and posterior results for LLB. The model minus observational data mismatches for the prior (blue dots) and posterior (red dots) results for the entire eight-year study period are shown in Figure 3b. The medians of data mismatches for the prior (blue line) and posterior (red line) results are shown for the January−March and October−December time periods. It is clear that the median of the three-month-modeled methane prior data (blue line) underestimates the observations (black line). This finding is consistent throughout the entire data record with each of the 16 three-monthly time periods showing similar underestimations. After optimization of the methane emissions in our inversion system, the discrepancy between the posterior-modeled methane data and observation (three-month median mismatch) is reduced from a range of −46 to −12 ppb using the prior-modeled data to a range of −15 to −3 ppb using the posterior-modeled data. The posterior results do not overshoot the observational results, and this suggests that our ensemble mean is likely closer to the lower bound of the emission estimates for Alberta and Saskatchewan. We find that our optimized results, although are improved significantly, do not fully capture all large mole fraction excursions in the observations (shown as below-zero red dots in Figure 3b). This can be partially explained by the data selection algorithm used (see Supporting Information S.7) to avoid biasing our results due to potential outliers in the observations.

The inversion optimization scheme adjusts the set of scaling factors to match the modeled results and observations. The goodness of match between the model and observations is a function of the number of scaling factors. With more scaling factors (i.e., number of subregions), the model−observation mismatch could be reduced. However, using a large number of scaling factors could result in overfitting the observations and sometimes yield unrealistic negative scaling factors. In this study, we found that solving for more than seven subregions did not yield statistically different Alberta and Saskatchewan total emission estimates from the results using four and seven subregions while these two setups did produce positive emissions in all subregions. In Figure 3b, the median biases shown as horizontal bars are minimal with ∼ −15 ppb being the most for one particular three-month period. In addition, large methane spikes are relatively infrequent. In the Supporting Information S.7 Data Selection section, we explained the details and reasons of data selection to avoid the impact of infrequent large excursions that could be the result of local sources and large transport model errors given that an optimization procedure would not be reliable in estimating such extreme CH_4 values.

An excerpt showing the individual prior- and posterior-modeled and observation time series records used in Figure 3b from November 1, 2015 to March 1, 2016 is shown in Figure 3a. The timing of the peaks in both the observations and the modeled outputs shown in Figure 3a shows a close correspondence and supports the argument that the largest contribution to the variability observed at LLB is caused by the transport of air masses that have accumulated emissions of methane from sources within our modeling domain. The yellow line shown in Figure 3a shows the contributions to the model data from the outer region (baseline). The outer region is the entire globe; see Supporting Information S.4 for details. The lack of variability in the baseline signal definitively shows that the enhanced peaks in methane measurements are primarily due to methane sources located in Alberta and Saskatchewan and not from sources in the other regions. The red shaded band shown in Figure 3a represents one standard deviation of the posterior results (red line) using the three

https://dx.doi.org/10.1021/acs.est.0c04117
Environ. Sci. Technol. 2020, 54, 14899−14909

inventory priors (Supporting Information S.5) and the two dispersion transport models. The observations are predominantly contained within this band of uncertainty. Figure 3c shows the frequency distributions of the observed methane data (black), as well as the prior (blue), posterior (red), and baseline (yellow) modeling data over the 2010−2017 period. The results underline the ability of the regional ensemble inversion system to produce optimized emissions to improve the match with observations.

Lastly, the Taylor diagram of the Pearson correlation coefficient and normalized standard deviation (NSD)[65] for the six possible combinations using three priors and the two transport models (see legend) is shown in Figure 3d for the seven-subregion configuration. NSD is defined as the standard deviation of prior- or posterior-modeled time series divided by the standard deviation of the observation time series. An NSD and correlation of 1 is the ideal statistical match. For LLB, the NSDs for all prior results using the different prior emissions and transport models are less than one, which further supports the point that the variability in the prior model mole fractions is underestimated and the source strengths in the inventories are too low in the surrounding area of the LLB site.

The same performance metric analyses showing observation and modeled prior and posterior time series for BRA, EST, and ETL, which are shown in Figure S9, display similar reductions in observation−model mismatch. At EST, the mismatch is reduced from a range of −52 to −25 ppb (prior) to −1 to +5 ppb (posterior), at BRA, the range is reduced from −26 to −21 ppb (prior) to −13 to −4 ppb (posterior), and at ETL, the range is reduced from −26 to −21 ppb (prior) to −17 to −12 ppb (posterior). For the Taylor diagrams, we find that the modeled mole fractions using the three prior emissions simulated by the same transport model are more distinguishable at BRA, EST, and ETL than at LLB. This indicates that these three sites are sensitive to differences in emissions in the inversion domain. Although the results tend to cluster together, there are differences that can be seen, particularly for the EST site. EST is located near the southern Alberta area, where the source strength suggested by P2[58] is considerably higher than the other two prior inventories. The differences introduced by the use of different transport models and prior emissions are similar. However, at the ETL site, the model results appear to be more sensitive to differences in transport models than differences in prior emissions. All four sites display NSDs of less than 1 for the priors, and NSDs for the optimized posterior emissions, on average, are approximately one, again indicating that the source strengths in the inventories are too low in the surrounding areas of all four sites and the optimization process produces smaller data−model mismatches.

INVERSION RESULTS AND DISCUSSION

Estimate of Anthropogenic Methane Emissions and Comparison to the National Inventory. Canada's NIR[5] provides greenhouse gas emission estimates on an annual basis. Because seasonal variations of emission estimates are small, the approach of doubling the six-month (January−March and October−December) study results to match the annual time frame of the NIR is considered to be reasonable. For oil and gas, the largest documented seasonal bias would be most likely associated with the use of chemical injection pumps in winter to prevent hydrate formation. The latest oil and gas methane inventory produced by Clearstone Engineering Ltd. for the Alberta Energy Regulator (2018) reported chemical injection pumps being used on about half the wells, which accounted for a small positive winter bias of 0.12 $MtCH_4$/year.[64] Monthly oil and gas production volumes are fairly consistent over the course of a year (National Energy Board[61,62]). For agriculture, there is a potential small negative winter bias with cattle populations being lower by 10% in winter than summer.[63] Because the reported waste emissions are so small, any potential seasonal biases in this source would be minor. These potential seasonal biases are all considered to be minor relative to the magnitude and uncertainty of our study results.

In Figure 4, the left bar summarizes the reported NIR emissions by year for energy (blue), agriculture (light blue), and waste (yellow) for Alberta and Saskatchewan. The NIR reports an annual mean emission rate of 2.3 $MtCH_4$ over the 2010−2017 time period. In this study, the annual mean (2010−2017) emission estimate in Alberta and Saskatchewan is 3.7 ± 0.7 $MtCH_4$, around 60% higher than the NIR reported annual mean (2010−2017) emission rate. This mean value is presented as a gray line in Figure 4. The uncertainty (estimated as one standard deviation of the ensemble results) of the eight-year ensemble mean is presented as a gray shaded area and includes the interannual variability of the estimates as well as the contributions of different ensemble components. It is important to note that the estimates for the individual subregions have much more variability, primarily due to the various spatial patterns in the prior emissions as shown in Figure S7. As such, we have more confidence in the reporting of the emission totals for Alberta and Saskatchewan together than the emissions for each individual subregion.

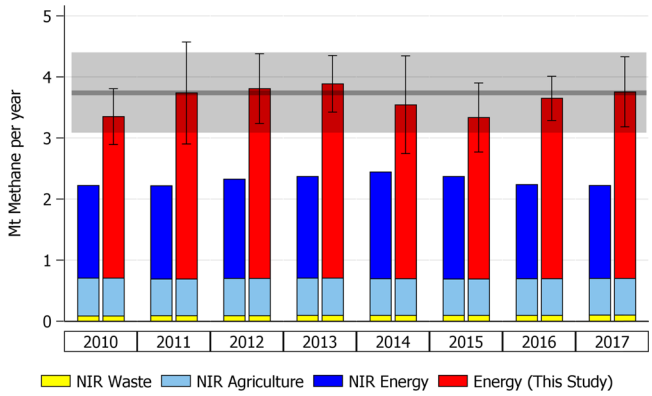

Figure 4. Annual model-derived and inventory emissions of methane in Alberta and Saskatchewan from 2010 to 2017. The annual NIR values for the energy, agriculture, and waste sectors are shown (left bar) in dark blue, light blue, and yellow, respectively. The top of the bar shown on the right represents the overall estimates from the model-based study. Shown in red are the energy (primarily oil and gas)-based emissions assuming that the NIR estimates for agriculture and waste are correct. The gray horizontal line shows the eight-year annual mean estimate. The light gray shaded band shows the ±1 SD of the 18 ensemble results.

A summary of the various inversion emission estimates using the three priors (P1, P2, and P3), the three model transports (ERA-FLEXPART and WRF-STILT with two different resolutions), and the four- and seven-subregion configurations is described in Supporting Information S.11. The range of the 18 individual inversion runs shows a maximum emission result for Alberta and Saskatchewan of 4.3 ± 0.6 $MtCH_4$/year (using the P2 prior and the ERA-FLEXPART transport model) and a

https://dx.doi.org/10.1021/acs.est.0c04117
Environ. Sci. Technol. 2020, 54, 14899−14909

minimum emission result of 3.0 ± 0.5 $MtCH_4$/year (using the P3 prior and the WRF-STILT transport model). One standard deviation of estimates using a given prior and a transport model for the eight-year study period is calculated to represent the uncertainty. A summary of the 18 inversions is presented in Table S4.

Source Categories Contributing to the Differences between Emission Estimates and NIR. There are four potential methane source categories that can contribute to the discrepancy between our results and the ECCC NIR: energy-related (oil and gas) sources, agricultural sources, waste sources, and natural emissions of methane from wetlands. Agriculture is a large source of methane in Alberta and Saskatchewan, contributing to ∼25% of the NIR-reported emissions. This source, however, is not likely the cause of the discrepancy. Emission estimates of methane from the NIR for agriculture have consistently been shown to be in line with the measurement study estimates. For example, atmospheric methane emission measurement studies carried out at feedlots in Alberta using open-path optical systems[66] as well as from aircraft platforms[67] have found results consistent with bottom-up methods. Furthermore, the NIR estimate can also rely on up-to-date statistical data, as animal populations (by animal type) are surveyed by Statistics Canada[63] twice per year (January and July). The National Inventory of agricultural methane provides an uncertainty range of −16% to +20%.[5] In addition, emission factors (IPCC Tier 2 and Tier 3) have also been closely studied[63,68] for ruminant emissions from beef in Canada, with results showing agreement, depending on cattle subcategories, to be within 13 and 20% for enteric sources. Lastly, there have been a number of studies conducted in Europe and the United States on agriculture sources that also show agreement within 20%.[69,70] Beef production in Canada is complex, and some facets of the emission cycle are most definitely better documented than others, but with so much available detailed industry information along with independent, atmospheric-based studies, we are confident that the NIR agriculture emission estimates are reasonable and that any potential reporting errors would be minimal considering the uncertainties in our analysis study. The NIR value for agriculture for each year is represented in our total as well and is shown in light blue in Figure 4.

Waste management procedures are a small source of methane in Alberta and Saskatchewan,[5] contributing to less than 5% of the NIR emissions. This source is not likely a cause of the discrepancy either even though many independent atmospheric studies show large ranges of emission estimates relative to inventories of −50% to +100%.[71−73] Due to its minor contribution, even with potential large reporting uncertainties, this source would not have an impact considering the uncertainty levels in this study. Similar to agriculture, the NIR value for waste for each year is represented in our total and is shown in yellow in Figure 4.

Wetlands are a significant source of methane in Canada in mid-summer but a near zero source in mid-winter.[27,28,37−39] The methane contribution of 0.2 ± 0.1 $MtCH_4$ for the six-month period used in this study was generated from the mean of optimized emissions over the period from 2010 to 2017 from CarbonTracker Europe-CH_4 (CTE-CH_4).[39] The contribution of wetland CH_4 emitted in October and November accounts for more than 95% of the total wetland emissions during the six-month period used in this study. CTE-CH_4[39] as well as other model outputs[27,28,37,38] reports negligible wetland emission amounts in Canada for the months of December to March. For comparison, we determined scaled annual emission amounts using different three-monthly time frames. The eight-year mean total emission amount for Alberta and Saskatchewan in our study using observational data for the three-month period from January to March (and scaled by 4), when wetland emissions are well accepted to be low, is 4.2 $MtCH_4$, which is within 15% of the scaled annual amount using observations from October to March. This clearly shows that wetland emission estimates in October and November do not contribute to significant uncertainties in our posterior estimates. Nonetheless, we slightly adjusted our annual results downward by 0.2 $MtCH_4$ to account for wetland methane emissions in October and November and thus provide a summary of the anthropogenic source activity only.

Since agriculture, waste, and natural sources are not likely the causes of the discrepancy as shown in Figure 4, we attribute the difference to energy-related (oil and gas) activities. Although our methane prior inventories do not allow direct conclusions about specific source sectors, it is important to note that the comparison of the prior emissions from energy sources between P1, P2, and P3 also shows the largest discrepancies, highlighting potential inconsistencies in the underlying activity data, emission factors, and/or missing oil and gas sources in the inventories (Supporting Information S.5).

According to Figure 4, the methane emission estimates for Alberta and Saskatchewan associated with energy (red bar) for each annual period from 2010 to 2017 are found to be notably higher than the NIR emission rate (left bar). An eight-year mean energy-sector source amount of 1.6 $MtCH_4$ is calculated from the NIR emissions, with a minimum of 1.5 $MtCH_4$ in 2010 and a maximum of 1.7 $MtCH_4$ in 2014. The annual emission estimate obtained in this study for Alberta and Saskatchewan indicates an eight-year mean energy source of 3.0 $MtCH_4$ with a minimum derived source amount of 2.8 $MtCH_4$ in 2015 and maximum of 3.4 $MtCH_4$ in 2017. Considering our eight-year ensemble uncertainty estimate of ±0.7 $MtCH_4$ in our analysis, we find that there is no statistical difference between any individual years (see overlapping error bars in Figure 4). With the supposition that emissions in Alberta and Saskatchewan from fossil fuel extraction and processing (i.e., oil and/or natural gas) are likely the main driver of the overall discrepancy between the model-based and NIR totals, this would lead to methane emissions from fossil fuel extraction and processing to be nearly twice the levels reported by Canada's national inventory for these two provinces (Figure 4). The additional methane emissions of 3.0−1.6 = 1.4 $MtCH_4$ equate to 35 $MtCO_2e$/year, using a global warming potential of 25, the same factor used in the NIR. This discrepancy of 35 $MtCO_2e$ would increase Canada's national annual methane estimate by about 40% for 2017.

This result suggests that systematic inconsistencies found using the smaller-scale, shorter-term studies in Lloydminster[20] may indeed affect the overall energy-related methane emissions in Alberta and Saskatchewan. Individual regions in Alberta and Saskatchewan were also previously reported to suffer from unreported venting emissions in that actual venting emissions were 2.5 ± 0.5 times higher than the values in the inventory.[20] Furthermore, our findings are generally consistent with the results from a larger-scale (hemispheric) methane inversion study that focused on the high northern latitudes (north of 50°N) and which estimated 4.3 ± 1.3 $MtCH_4$/year of

https://dx.doi.org/10.1021/acs.est.0c04117
Environ. Sci. Technol. 2020, 54, 14899−14909

anthropogenic emissions for Alberta.[27] More analyses of the effects of different ensemble members (or settings) and robustness of the inversion results are shown in Supporting Information S.11.

Implications. This study and other studies in Alberta, British Columbia, and the United States suggest that methane emissions from oil and gas activities in North America are substantially higher (ranging from 50 to 200%) than the amounts reported in the national inventories. Although the ensemble inversion system used in this study cannot fully assess the interannual variability of emissions, it does provide insights into the provincial-level methane reporting and it provides a useful complementary tool for detecting long-term step changes such as the anticipated 40−45% reduction in methane emissions from the oil and gas sector and evaluating the effectiveness of methane regulations once implemented.

The discrepancy between these results for Alberta and Saskatchewan and the NIR reflects the difference in scope since the oil and gas industries are required to report the methane activity information only from known processes (flaring, venting, etc.) and have reporting minimums below which reporting is not required. Emissions from various fugitive and unintended processes are broadly considered under-reported or underestimated. For example, methane emissions from storage tanks are a relatively minor source in inventories, but recent studies have suggested that the contribution from tanks may be higher.[42] In addition, it has been documented that "super-emitters" (i.e., equipment at facilities that leak many times higher emissions than average leaking equipment) exist in the upstream oil and gas (UOG) industry, but the frequency and magnitude of these "super-emitters" are not well understood.[58,74,75] Atmospheric observation-based approaches have the potential to reflect all emission sources.

Ongoing reconciliation of the discrepancies between atmospheric observations and modeled (top-down) assessments and those obtained by inventory (bottom-up) protocols will be useful to combine both in a complementary fashion. This requires increasing the number and density of atmospheric measurements sites and improvements in inverse modeling capabilities, in parallel with the ongoing developments in national inventory bottom-up reporting methods. A closer integration of both approaches can provide greater confidence in emission reporting. Sustained and/or strengthened hourly methane atmospheric monitoring with increased modeling system capabilities[24,28] to estimate emissions can provide additional information and insights to guide mitigation planning and assess ongoing progress toward meeting emission reduction goals. Such a system to manage and report emissions should reflect the advances in inventory estimation methodologies, as suggested by the 2019 refinement of the 2006 IPCC guidelines.[76]

■ ASSOCIATED CONTENT

Supporting Information

The Supporting Information is available free of charge at https://pubs.acs.org/doi/10.1021/acs.est.0c04117.

Details of the site descriptions, measurement systems, transport models, baseline estimations, prior emissions, inversion spatial configurations, data selection, Bayesian model, and AQ2013 methane prior emissions (PDF)

■ AUTHOR INFORMATION

Corresponding Author

Douglas E. J. Worthy − *Climate Research Division, Environment and Climate Change Canada, Toronto, Ontario M3H 5T4, Canada*; Phone: 1 416 797 5169; Email: doug.worthy@canada.ca

Authors

Elton Chan − *Climate Research Division, Environment and Climate Change Canada, Toronto, Ontario M3H 5T4, Canada*

Douglas Chan − *Climate Research Division, Environment and Climate Change Canada, Toronto, Ontario M3H 5T4, Canada*

Misa Ishizawa − *Climate Research Division, Environment and Climate Change Canada, Toronto, Ontario M3H 5T4, Canada*

Michael D. Moran − *Air Quality Research Division, Environment and Climate Change Canada, Toronto, Ontario M3H 5T4, Canada*

Andy Delcloo − *Royal Meteorological Institute of Belgium, B-1180 Brussels, Belgium*

Felix Vogel − *Climate Research Division, Environment and Climate Change Canada, Toronto, Ontario M3H 5T4, Canada*

Complete contact information is available at: https://pubs.acs.org/10.1021/acs.est.0c04117

Author Contributions

The manuscript was written through contributions of all authors. All authors have given approval to the final manuscript.

Notes

The authors declare no competing financial interest.

■ ACKNOWLEDGMENTS

The authors would like to thank Dr. Junhua Zhang of the Air Quality Research Division at ECCC for the development of the AQ2013 methane emission map for Canada, Drs. Owen R. Cooper and Jerome Brioude for providing valuable support in setting up the FLEXPART model, Dr. Yuehua Wu for the implementation of the MCMC method, and Dr. Aki Tsuruta for providing eight years of optimized wetland emission data as part of the CarbonTracker Europe-CH_4 (CTE-CH_4) project. Credit of producing Figure 2a is given to Terry Steinkey of Map Town. We also appreciate the support of the CarbonTracker-Lagrange (CT-L) program team at NOAA in Boulder for providing the WRF-STILT footprint data. The authors particularly wish to extend their gratitude to Dr. John Basarab at the Agriculture and Rural Development Research Centre in Lacombe, AB and Dr. Ray Desjardin at Agriculture and Agri-Food Canada in Ottawa, ON for their valuable discussions, insights, and input on agricultural sources of methane from cattle. Finally, we greatly appreciate comments on the manuscript from Marjorie Shepherd of ECCC's Climate Research Division, John Liggio of ECCC's Air Quality Research Division, and Steve Smyth and Dominique Blain of ECCC"s Pollutant Inventories and Reporting Division.

REFERENCES

(1) Gasser, T.; Peters, G. P.; Fuglestvedt, J. S.; Collins, W. J.; Shindell, D. T.; Ciais, P. Accounting for the Climate-Carbon Feedback in Emission Metric. *Earth Syst. Dyn.* **2017**, *8*, 235−253.

(2) *UNFCCC. The Paris Agreement | UNFCCC* https://unfccc.int/process-and-meetings/the-paris-agreement/the-paris-agreement (accessed Apr 1, 2020).

(3) Government of Canada. *Technical Backgrounder: Federal methane regulations for the upstream oil and gas sector - Canada.ca* https://www.canada.ca/en/environment-climate-change/news/2018/04/federal-methane-regulations-for-the-upstream-oil-and-gas-sector.html (accessed Jun 28, 2019).

(4) Government of Canada. *Regulations Respecting Reduction in the Release of Methane and Certain Volatile Organic Compounds* https://laws-lois.justice.gc.ca/PDF/SOR-2018-66.pdf (accessed Jun 28, 2019).

(5) *Environment Canada. National Inventory Report: Greenhouse gas sources and sinks in Canada* http://www.publications.gc.ca/site/eng/9.506002/publication.html (accessed Jan 9, 2020).

(6) IPCC. 2006 *IPCC Guidelines for National Greenhouse Gas Inventories — IPCC* https://www.ipcc.ch/report/2006-ipcc-guidelines-for-national-greenhouse-gas-inventories/ (accessed Apr 1, 2020).

(7) IPCC. 2019 *Refinement to the 2006 IPCC Guidelines for National Greenhouse Gas Inventories — IPCC* https://www.ipcc.ch/report/2019-refinement-to-the-2006-ipcc-guidelines-for-national-greenhouse-gas-inventories/ (accessed Apr 1, 2020).

(8) Allen, D. T.; Torres, V. M.; Thomas, J.; Sullivan, D. W.; Harrison, M.; Hendler, A.; Herndon, S. C.; Kolb, C. E.; Fraser, M. P.; Hill, A. D.; Lamb, B. K.; Miskimins, J.; Sawyer, R. F.; Seinfeldi, J. H. Measurements of Methane Emissions at Natural Gas Production Sites in the United States. *Proc. Natl. Acad. Sci. U. S. A.* **2013**, *110*, 17768−17773.

(9) Brandt, A. R.; Heath, G. A.; Kort, E. A.; O'Sullivan, F.; Pétron, G.; Jordaan, S. M.; Tans, P.; Wilcox, J.; Gopstein, A. M.; Arent, D.; Wofsy, S.; Brown, N. J.; Bradley, R.; Stucky, G. D.; Eardley, D.; Harriss, R. Methane Leaks from North American Natural Gas Systems. *Science* **2014**, *343*, 733−735.

(10) Chambers, A. K.; Strosher, M.; Wootton, T.; Moncrieff, J.; McCready, P. Direct Measurement of Fugitive Emissions of Hydrocarbons from a Refinery. *J. Air Waste Manag. Assoc.* **2008**, *58*, 1047−1056.

(11) Karion, A.; Sweeney, C.; Pétron, G.; Frost, G.; Michael Hardesty, R.; Kofler, J.; Miller, B. R.; Newberger, T.; Wolter, S.; Banta, R.; Brewer, A.; Dlugokencky, E.; Lang, P.; Montzka, S. A.; Schnell, R.; Tans, P.; Trainer, M.; Zamora, R.; Conley, S. Methane Emissions Estimate from Airborne Measurements over a Western United States Natural Gas Field. *Geophys. Res. Lett.* **2013**, *40*, 4393−4397.

(12) Katzenstein, A. S.; Doezema, L. A.; Simpson, I. J.; Blake, D. R.; Rowland, F. S. Extensive Regional Atmospheric Hydrocarbon Pollution in the Southwestern United States. *Proc. Natl. Acad. Sci. U. S. A.* **2003**, *100*, 11975−11979.

(13) Miller, S. M.; Wofsy, S. C.; Michalak, A. M.; Kort, E. A.; Andrews, A. E.; Biraud, S. C.; Dlugokencky, E. J.; Eluszkiewicz, J.; Fischer, M. L.; Janssens-Maenhout, G.; Miller, B. R.; Miller, J. B.; Montzka, S. A.; Nehrkorn, T.; Sweeney, C. Anthropogenic Emissions of Methane in the United States. *Proc. Natl. Acad. Sci. U. S. A.* **2013**, *110*, 20018−20022.

(14) Pétron, G.; Frost, G.; Miller, B. R.; Hirsch, A. I.; Montzka, S. A.; Karion, A.; Trainer, M.; Sweeney, C.; Andrews, A. E.; Miller, L.; Kofler, J.; Bar-Ilan, A.; Dlugokencky, E. J.; Patrick, L.; Moore, C. T.; Ryerson, T. B.; Siso, C.; Kolodzey, W.; Lang, P. M.; Conway, T.; Novelli, P.; Masarie, K.; Hall, B.; Guenther, D.; Kitzis, D.; Miller, J.; Welsh, D.; Wolfe, D.; Neff, W.; Tans, P. Hydrocarbon Emissions Characterization in the Colorado Front Range: A Pilot Study. *J. Geophys. Res. Atmos.* **2012**, *117*, D04304.

(15) Pétron, G.; Karion, A.; Sweeney, C.; Miller, B. R.; Montzka, S. A.; Frost, G. J.; Trainer, M.; Tans, P.; Andrews, A.; Kofler, J.; Helmig, D.; Guenther, D.; Dlugokencky, E.; Lang, P.; Newberger, T.; Wolter, S.; Hall, B.; Novelli, P.; Brewer, A.; Conley, S.; Hardesty, M.; Banta, R.; White, A.; Noone, D.; Wolfe, D.; Schnell, R. A New Look at Methane and Nonmethane Hydrocarbon Emissions from Oil and Natural Gas Operations in the Colorado Denver-Julesburg Basin. *J. Geophys. Res.* **2014**, *119*, 6836−6852.

(16) Barkley, Z. R.; Davis, K. J.; Feng, S.; Balashov, N.; Fried, A.; DiGangi, J.; Choi, Y.; Halliday, H. S. Forward Modeling and Optimization of Methane Emissions in the South Central United States Using Aircraft Transects Across Frontal Boundaries. *Geophys. Res. Lett.* **2019**, *46*, 13564−13573.

(17) GreenPath Energy Ltd. *GreenPath 2016 Alberta Fugitive and Vented Emissions Inventory Study*; 2016.

(18) Baray, S.; Darlington, A.; Gordon, M.; Hayden, K. L.; Leithead, A.; Li, S. M.; Liu, P. S. K.; Mittermeier, R. L.; Moussa, S. G.; O'Brien, J.; Staebler, R.; Wolde, M.; Worthy, D.; McLaren, R. Quantification of Methane Sources in the Athabasca Oil Sands Region of Alberta by Aircraft Mass Balance. *Atmos. Chem. Phys.* **2018**, *18*, 7361−7378.

(19) O'Connell, E.; Risk, D.; Atherton, E.; Bourlon, E.; Fougère, C.; Baillie, J.; Lowry, D.; Johnson, J. Methane Emissions from Contrasting Production Regions within Alberta, Canada: Implications under Incoming Federal Methane Regulations. *Elementa* **2019**, *7*, 3.

(20) Johnson, M. R.; Tyner, D. R.; Conley, S.; Schwietzke, S.; Zavala-Araiza, D. Comparisons of Airborne Measurements and Inventory Estimates of Methane Emissions in the Alberta Upstream Oil and Gas Sector. *Environ. Sci. Technol.* **2017**, *51*, 13008−13017.

(21) Bergamaschi, P.; Krol, M.; Dentener, F.; Vermeulen, A.; Meinhardt, F.; Graul, R.; Ramonet, M.; Peters, W.; Dlugokencky, E. J. Inverse Modelling of National and European CH_4 Emissions Using the Atmospheric Zoom Model TM5. *Atmos. Chem. Phys.* **2005**, *5*, 2431−2460.

(22) Bergamaschi, P.; Krol, M.; Meirink, J. F.; Dentener, F.; Segers, A.; Van Aardenne, J.; Monni, S.; Vermeulen, A. T.; Schmidt, M.; Ramonet, M.; Yver, C.; Meinhardt, F.; Nisbet, E. G.; Fisher, R. E.; O'Doherty, S.; Dlugokencky, E. J. Inverse Modeling of European CH4 Emissions 2001-2006. *J. Geophys. Res. Atmos.* **2010**, *115*, D22309.

(23) Bergamaschi, P.; Corazza, M.; Karstens, U.; Athanassiadou, M.; Thompson, R. L.; Pison, I.; Manning, A. J.; Bousquet, P.; Segers, A.; Vermeulen, A. T.; Janssens-Maenhout, G.; Schmidt, M.; Ramonet, M.; Meinhardt, F.; Aalto, T.; Haszpra, L.; Moncrieff, J.; Popa, M. E.; Lowry, D.; Steinbacher, M.; Jordan, A.; O'Doherty, S.; Piacentino, S.; Dlugokencky, E. Top-down Estimates of European CH4 and N2O Emissions Based on Four Different Inverse Models. *Atmos. Chem. Phys.* **2015**, *15*, 715−736.

(24) Bergamaschi, P.; Karstens, U.; Manning, A. J.; Saunois, M.; Tsuruta, A.; Berchet, A.; Vermeulen, A. T.; Arnold, T.; Janssens-Maenhout, G.; Hammer, S.; Levin, I.; Schmidt, M.; Ramonet, M.; Lopez, M.; Lavric, J.; Aalto, T.; Chen, H.; Feist, D. G.; Gerbig, C.; Haszpra, L.; Hermansen, O.; Manca, G.; Moncrieff, J.; Meinhardt, F.; Necki, J.; Galkowski, M.; O'Doherty, S.; Paramonova, N.; Scheeren, H. A.; Steinbacher, M.; Dlugokencky, E. Inverse Modelling of European CH4 Emissions during 2006-2012 Using Different Inverse Models and Reassessed Atmospheric Observations. *Atmos. Chem. Phys.* **2018**, *18*, 901−920.

(25) Cressot, C.; Chevallier, F.; Bousquet, P.; Crevoisier, C.; Dlugokencky, E. J.; Fortems-Cheiney, A.; Frankenberg, C.; Parker, R.; Pison, I.; Scheepmaker, R. A.; Montzka, S. A.; Krummel, P. B.; Steele, L. P.; Langenfelds, R. L. On the Consistency between Global and Regional Methane Emissions Inferred from SCIAMACHY, TANSO-FTS, IASI and Surface Measurements. *Atmos. Chem. Phys.* **2014**, *14*, 577−592.

(26) Manning, A. J.; O'Doherty, S.; Jones, A. R.; Simmonds, P. G.; Derwent, R. G. Estimating UK Methane and Nitrous Oxide Emissions from 1990 to 2007 Using an Inversion Modeling Approach. *J. Geophys. Res. Atmos.* **2011**, *116*, D02305.

(27) Thompson, R. L.; Sasakawa, M.; Machida, T.; Aalto, T.; Worthy, D.; Lavric, J. V.; Myhre, C. L.; Stohl, A. Methane Fluxes in the High Northern Latitudes for 2005-2013 Estimated Using a

https://dx.doi.org/10.1021/acs.est.0c04117
Environ. Sci. Technol. 2020, 54, 14899−14909

Bayesian Atmospheric Inversion. *Atmos. Chem. Phys.* **2017**, *17*, 3553−3572.
(28) Bergamaschi, P.; Danila, A.; Weiss, R. F.; Ciais, P.; Thompson, R. L.; Brunner, D.; Levin, I.; Meijer, Y.; Chevallier, F.; Bovensmann, H.; Crisp, D.; Basu, S.; Dlugokencky, E.; Engelen, R.; Gerbig, C.; Günther, D.; Hammer, S.; Henne, S.; Houweling, S.; Peylin, P.; Pinty, B.; Ramonet, M.; Reimann, S.; Röckmann, T.; Schmidt, M.; Strogies, M.; Sussams, J.; Tarasova, O.; Aardenne, J. V.; Vermeulen, A. T.; Vogel, F. *Atmospheric Monitoring and Inverse Modelling for Verification of Greenhouse Gas Inventories*; 2018. 10. 2760/02681.
(29) Tolk, L. F.; Dolman, A. J.; Meesters, A. G. C. A.; Peters, W. A Comparison of Different Inverse Carbon Flux Estimation Approaches for Application on a Regional Domain. *Atmos. Chem. Phys.* **2011**, *11*, 10349−10365.
(30) Stohl, A.; Seibert, P.; Arduini, J.; Eckhardt, S.; Fraser, P.; Greally, B. R.; Lunder, C.; Maione, M.; Mühle, J.; O'Doherty, S.; Prinn, R. G.; Reimann, S.; Saito, T.; Schmidbauer, N.; Simmonds, P. G.; Vollmer, M. K.; Weiss, R. F.; Yokouchi, Y. An Analytical Inversion Method for Determining Regional and Global Emissions of Greenhouse Gases: Sensitivity Studies and Application to Halocarbons. *Atmos. Chem. Phys.* **2009**, *9*, 1597−1620.
(31) Brioude, J.; Kim, S. W.; Angevine, W. M.; Frost, G. J.; Lee, S. H.; McKeen, S. A.; Trainer, M.; Fehsenfeld, F. C.; Holloway, J. S.; Ryerson, T. B.; Williams, E. J.; Petron, G.; Fast, J. D. Top-down Estimate of Anthropogenic Emission Inventories and Their Interannual Variability in Houston Using a Mesoscale Inverse Modeling Technique. *J. Geophys. Res. Atmos.* **2011**, *116*, D20305.
(32) Gerbig, C.; Lin, J. C.; Wofsy, S. C.; Daube, B. C.; Andrews, A. E.; Stephens, B. B.; Bakwin, P. S.; Grainger, C. A. Toward Constraining Regional-Scale Fluxes of CO2 with Atmospheric Observations over a Continent: 1. Observed Spatial Variability from Airborne Platforms. *J. Geophys. Res. D Atmos.* **2003**, *108* (). DOI: 10.1029/2002jd003018.
(33) Kort, E. A.; Eluszkiewicz, J.; Stephens, B. B.; Miller, J. B.; Gerbig, C.; Nehrkorn, T.; Daube, B. C.; Kaplan, J. O.; Houweling, S.; Wofsy, S. C. Emissions of CH4 and N2O over the United States and Canada Based on a Receptor-Oriented Modeling Framework and COBRA-NA Atmospheric Observations. *Geophys. Res. Lett.* **2008**, *35*, L18808.
(34) Jeong, S.; Zhao, C.; Andrews, A. E.; Bianco, L.; Wilczak, J. M.; Fischer, M. L. Seasonal Variation of CH4 Emissions from Central California. *J. Geophys. Res. Atmos.* **2012**, *117*, D11306.
(35) Zhao, C.; Andrews, A. E.; Bianco, L.; Eluszkiewicz, J.; Hirsch, A.; MacDonald, C.; Nehrkorn, T.; Fischer, M. L. Atmospheric Inverse Estimates of Methane Emissions from Central California. *J. Geophys. Res. Atmos.* **2009**, *114*, D16302.
(36) Worthy, D. E. J.; Trivett, N. B. A.; Hopper, J. F.; Bottenheim, J. W.; Levin, I. Analysis of Long-Range Transport Events at Alert, Northwest Territories, during the Polar Sunrise Experiments. *J. Geophys. Res.* **1994**, *99*, 25329.
(37) Ishizawa, M.; Chan, D.; Worthy, D.; Chan, E.; Vogel, F.; Maksyutov, S. Analysis of Atmospheric CH4 in Canadian Arctic and Estimation of the Regional CH4 Fluxes. *Atmos. Chem. Phys.* **2019**, *19*, 4637−4658.
(38) Anthony Bloom, A.; Bowman, W. K.; Lee, M.; Turner, J. A.; Schroeder, R.; Worden, R. J.; Weidner, R.; McDonald, C. K.; Jacob, J. D. A Global Wetland Methane Emissions and Uncertainty Dataset for Atmospheric Chemical Transport Models (WetCHARTs Version 1.0). *Geosci. Model Dev.* **2017**, *10*, 2141−2156.
(39) Tsuruta, A.; Aalto, T.; Backman, L.; Hakkarainen, J.; Van Der Laan-Luijkx, I. T.; Krol, M. C.; Spahni, R.; Houweling, S.; Laine, M.; Dlugokencky, E.; Gomez-Pelaez, A. J.; Van Der Schoot, M.; Langenfelds, R.; Ellul, R.; Arduini, J.; Apadula, F.; Gerbig, C.; Feist, D. G.; Kivi, R.; Yoshida, Y.; Peters, W. Global Methane Emission Estimates for 2000-2012 from CarbonTracker Europe-CH4 v1.0. *Geosci. Model Dev.* **2017**, *10*, 1261−1289.
(40) *CanFax. CanFax* http://www.canfax.ca/Main.aspx(accessed Jul 8, 2019).
(41) Stohl, A.; Forster, C.; Frank, A.; Seibert, P.; Wotawa, G. Technical Note: The Lagrangian Particle Dispersion Model FLEXPART Version 6.2. *Atmos. Chem. Phys.* **2005**, *5*, 2461−2474.
(42) Lyon, D. R.; Alvarez, R. A.; Zavala-Araiza, D.; Brandt, A. R.; Jackson, R. B.; Hamburg, S. P. Aerial Surveys of Elevated Hydrocarbon Emissions from Oil and Gas Production Sites. *Environ. Sci. Technol.* **2016**, *50*, 4877−4886.
(43) Rowe, D.; Muehlenbachs, K. Isotopic Fingerprints of Shallow Gases in the Western Canadian Sedimentary Basin: Tools for Remediation of Leaking Heavy Oil Wells. *Org. Geochem.* **1999**, *30*, 861−871.
(44) Watson, T. L.; Bachu, S. Evaluation of the Potential for Gas and CO2 Leakage along Wellbores. *SPE Drilling and Completion*. Society of Petroleum Engineers: Galveston, Texas, U.S.A. 2009, 115−126. DOI: 10.2118/106817-PA.
(45) Lin, J. C.; Gerbig, C.; Wofsy, S. C.; Andrews, A. E.; Daube, B. C.; Davis, K. J.; Grainger, C. A. A. Near-Field Tool for Simulating the Upstream Influence of Atmospheric Observations: The Stochastic Time-Inverted Lagrangian Transport (STILT) Model. *J. Geophys. Res. D Atmos.* **2003**, *108*, ACH 2-1−ACH 2-17.
(46) Lin, J. C.; Gerbig, C. Accounting for the Effect of Transport Errors on Tracer Inversions. *Geophys. Res. Lett.* **2005**, *32*, 1−5.
(47) Uppala, S. M.; Kållberg, P. W.; Simmons, A. J.; Andrae, U.; da Costa Bechtold, V.; Fiorino, M.; Gibson, J. K.; Haseler, J.; Hernandez, A.; Kelly, G. A.; Li, X.; Onogi, K.; Saarinen, S.; Sokka, N.; Allan, R. P.; Andersson, E.; Arpe, K.; Balmaseda, M. A.; Beljaars, A. C. M.; van de Berg, L.; Bidlot, J.; Bormann, N.; Caires, S.; Chevallier, F.; Dethof, A.; Dragosavac, M.; Fisher, M.; Fuentes, M.; Hagemann, S.; Hólm, E.; Hoskins, B. J.; Isaksen, L.; Janssen, P. A. E. M.; Jenne, R.; McNally, A. P.; Mahfouf, J. F.; Morcrette, J. J.; Rayner, N. A.; Saunders, R. W.; Simon, P.; Sterl, A.; Trenberth, K. E.; Untch, A.; Vasiljevic, D.; Viterbo, P.; Woollen, J. The ERA-40 Re-Analysis. *Q. J. R. Meteorol. Soc.* **2005**, *131*, 2961−3012.
(48) Dee, D. P.; Uppala, S. M.; Simmons, A. J.; Berrisford, P.; Poli, P.; Kobayashi, S.; Andrae, U.; Balmaseda, M. A.; Balsamo, G.; Bauer, P.; Bechtold, P.; Beljaars, A. C. M.; van de Berg, L.; Bidlot, J.; Bormann, N.; Delsol, C.; Dragani, R.; Fuentes, M.; Geer, A. J.; Haimberger, L.; Healy, S. B.; Hersbach, H.; Hólm, E. V.; Isaksen, L.; Kållberg, P.; Köhler, M.; Matricardi, M.; Mcnally, A. P.; Monge-Sanz, B. M.; Morcrette, J. J.; Park, B. K.; Peubey, C.; de Rosnay, P.; Tavolato, C.; Thépaut, J. N.; Vitart, F. The ERA-Interim Reanalysis: Configuration and Performance of the Data Assimilation System. *Q. J. R. Meteorol. Soc.* **2011**, *137*, 553−597.
(49) Skamarock, W. C.; Klemp, J. B.; Dudhia, J.; Gill, D. O.; Liu, Z.; Berner, J.; Wang, W.; Powers, J. G.; Duda, M. G.; Barker, D. M.; Huang, X.-Y. A. *Description of the Advanced Research WRF Version 4. NCAR Tech. Note NCAR/TN-556+STR*, 145. 2019, 145 . DOI: 10.5065/1dfh-6p97.
(50) ESRL. ESRL Global Monitoring *Division-Global Greenhouse Gas Reference Network* https://www.esrl.noaa.gov/gmd/ccgg/carbontracker-lagrange/ (accessed Dec 16, 2019).
(51) Belikov, D. A.; Maksyutov, S.; Sherlock, V.; Aoki, S.; Deutscher, N. M.; Dohe, S.; Griffith, D.; Kyro, E.; Morino, I.; Nakazawa, T.; Notholt, J.; Rettinger, M.; Schneider, M.; Sussmann, R.; Toon, G. C.; Wennberg, P. O.; Wunch, D. Simulations of Column-Averaged CO2 and CH4 Using the NIES TM with a Hybrid Sigma-Isentropic (σ-θ) Vertical Coordinate. *Atmos. Chem. Phys.* **2013**, *13*, 1713−1732.
(52) Etiope, G. *Natural Gas Seepage: The Earth's Hydrocarbon Degassing*; Springer International Publishing, 2015. DOI: 10.1007/978-3-319-14601-0.
(53) Etiope, G.; Ciotoli, G.; Schwietzke, S.; Schoell, M. Gridded Maps of Geological Methane Emissions and Their Isotopic Signature. *Earth Syst. Sci. Data* **2019**, *11*, 1−22.
(54) Dickson, R. J.; Oliver, W. R. Emissions Models for Regional Air Quality Studies. *Environ. Sci. Technol.* **1991**, *25*, 1533−1535.
(55) Houyoux, M. R.; Vukovich, J. M.; Coats, C. J., Jr.; Wheeler, N. J. M.; Kasibhatla, P. S. Emission Inventory Development and Processing for the Seasonal Model for Regional Air Quality (SMRAQ) Project. *J. Geophys. Res. Atmos.* **2000**, *105*, 9079−9090.

(56) Pouliot, G.; Pierce, T.; Denier van der Gon, H.; Schaap, M.; Moran, M.; Nopmongcol, U. Comparing Emission Inventories and Model-Ready Emission Datasets between Europe and North America for the AQMEII Project. *Atmos. Environ.* **2012**, *53*, 4−14.
(57) Moran, M. D.; Dastoor, A.; Morneau, G. Long-Range Transport of Air Pollutants and Regional and Global Air Quality Modelling. *Air Qual. Manag. Can. Perspect. A Glob. Issue* **2014**, *9789400775*, 69−98.
(58) Sheng, J. X.; Jacob, D. J.; Maasakkers, J. D.; Sulprizio, M. P.; Zavala-Araiza, D.; Hamburg, S. P. A High-Resolution (0.1° × 0.1°) Inventory of Methane Emissions from Canadian and Mexican Oil and Gas Systems. *Atmos. Environ.* **2017**, *158*, 211−215.
(59) Olivier, J. G. J.; Bouwman, A. F.; Van Der Maas, C. W. M.; Berdowski, J. J. M. *Emission database for global atmospheric research (EDGAR): Version 2.0* http://edgar.jrc.ec.europa.eu. DOI: 10.1016/S0166-1116(06)80262-1.
(60) Kass, R. E.; Gilks, W. R.; Richardson, S.; Spiegelhalter, D. J. *Markov Chain Monte Carlo in Practice.*; Gilks, W. R., Spiegelhalter, D. J., Richardson, S., Ed.; Chapman and Hall/CRC, 1997; *92*. DOI: 10.2307/2965438.
(61) *NEB. Marketable natural gas production in Canada* http://www.neb-one.gc.ca/clf-nsi/rnrgynfmtn/sttstc/mrktblntrlgsprdctn/mrktblntrlgsprdctn-eng.html(accessed Sep 3, 2019).
(62) Budgell, P.. *Estimated Production of Canadian Crude Oil and Equivalent* https://www.neb-one.gc.ca/nrg/sttstc/crdlndptrlmprdct/stt/stmtdprdctn-eng.html# (accessed Sep 3, 2019).
(63) Government of Canada, S. C. *CANSIM - 003-0032 - Number of cattle, by class and farm type* http://www5.statcan.gc.ca/cansim/a05?lang=eng&id=0030032&pattern=0030032&searchTypeByValue=1&p2=35 (accessed Sep 3, 2019).
(64) Clearstone Eng. Ltd. *Inventory of Atmospheric Emissions from Heavy Oil Production Facilities in the Three Creeks Area*; 2015.
(65) Taylor, K. E. Summarizing Multiple Aspects of Model Performance in a Single Diagram. *J. Geophys. Res. Atmos.* **2001**, *106*, 7183−7192.
(66) Van Haarlem, R. P.; Desjardins, R. L.; Gao, Z.; Flesch, T. K.; Li, X. Methane and Ammonia Emissions from a Beef Feedlot in Western Canada for a Twelve-Day Period in the Fall. *Can. J. Anim. Sci.* **2008**, *88*, 641−649.
(67) Desjardins, R. L.; Worth, D.; Pattey, E.; Mauder, M.; Srinivasan, R.; Worthy, D.; Sweeney, C.; Metzger, S. *Airborne Flux Measurement of Agricultural Methane Emissions*. First AMS Conference on Atmospheric Biogeosciences. AMS May 29, 2012, J4.5.
(68) Karimi-Zindashty, Y.; MacDonald, J. D.; Desjardins, R. L.; Worth, D. E.; Hutchinson, J. J.; Vergé, X. P. C. Sources of Uncertainty in the IPCC Tier 2 Canadian Livestock Model. *J. Agric. Sci.* **2012**, *150*, 556−569.
(69) Henne, S.; Brunner, D.; Oney, B.; Leuenberger, M.; Eugster, W.; Bamberger, I.; Meinhardt, F.; Steinbacher, M.; Emmenegger, L. Validation of the Swiss Methane Emission Inventory by Atmospheric Observations and Inverse Modelling. *Atmos. Chem. Phys.* **2016**, *16*, 3683−3710.
(70) Hristov, A. N.; Harper, M.; Meinen, R.; Day, R.; Lopes, J.; Ott, T.; Venkatesh, A. A. Randles, C. Discrepancies and Uncertainties in Bottom-up Gridded Inventories of Livestock Methane Emissions for the Contiguous United States. *Environ. Sci. Technol.* **2017**, *51*, 13668−13677.
(71) Cusworth, D. H.; Duren, R.; Thorpe, A. K.; Tseng, E.; Thompson, D.; Guha, A.; Newman, S.; Foster, K.; Miller, C. E. Using Remote Sensing to Detect, Validate, and Quantify Methane Emissions from California Solid Waste Operations. *Environ. Res. Lett.* **2020**, *15*, No. 054012.
(72) Mønster, J.; Samuelsson, J.; Kjeldsen, P.; Scheutz, C. Quantification of Methane Emissions from 15 Danish Landfills Using the Mobile Tracer Dispersion Method. *Waste Manage.* **2015**, *35*, 177−186.
(73) Mønster, J.; Kjeldsen, P.; Scheutz, C. Methodologies for Measuring Fugitive Methane Emissions from Landfills − A Review. *Waste Manage.* **2019**, *87*, 835−859 Elsevier Ltd March 15, 2019.
(74) Maasakkers, J. D.; Jacob, D. J.; Sulprizio, M. P.; Turner, A. J.; Weitz, M.; Wirth, T.; Hight, C.; DeFigueiredo, M.; Desai, M.; Schmeltz, R.; Hockstad, L.; Bloom, A. A.; Bowman, K. W.; Jeong, S.; Fischer, M. L. Gridded National Inventory of U.S. Methane Emissions. *Environ. Sci. Technol.* **2016**, *50*, 13123−13133.
(75) Zavala-Araiza, D.; Alvarez, R. A.; Lyon, D. R.; Allen, D. T.; Marchese, A. J.; Zimmerle, D. J.; Hamburg, S. P. Super-Emitters in Natural Gas Infrastructure Are Caused by Abnormal Process Conditions. *Nat. Commun.* **2017**, *8*, 14012.
(76) Gitarskiy, M. L. *The Refinement To the 2006 Ipcc Guidelines for National Greenhouse Gas Inventories* https://www.ipcc.ch/report/2019-refinement-to-the-2006-ipcc-guidelines-for-national-greenhouse-gas-inventories/ (accessed Sep 3, 2019). DOI: 10.21513/0207-2564-2019-2-05-13.

https://dx.doi.org/10.1021/acs.est.0c04117
Environ. Sci. Technol. 2020, 54, 14899−14909